J. Fluid Mech. (1993), *vol.* 255, *pp.* 323–347

Oscillations in the near field of a heated two-dimensional jet

By MING-HUEI YU† AND PETER A. MONKEWITZ‡
Department of Mechanical, Aerospace and Nuclear Engineering, University of California, Los Angeles, CA 90024-1597, USA

(Received 10 July 1992 and in revised form 17 April 1993)

A two-dimensional hot-air jet is investigated experimentally in the transitional regime. The density effect on the near-field behaviour of the initially laminar jet is explored by flow visualization, mean flow measurements and spectral analysis of fluctuating data. It is shown that the broadband amplitude spectra which characterize cold jets become line-dominated for hot jets when the ratio of the jet-exit to the ambient density is below approximately 0.9. Below this critical density ratio the oscillations in the hot jet are shown to be self-excited. That is, the onset of the global oscillations is identified as a Hopf bifurcation and the critical parameter is determined from amplitude spectra and autobicoherence, with the latter proving to be more reliable. Furthermore, the development of three-dimensional structures, which contribute to the jet spreading, is revealed by flow visualization. It is found that, for the parameters investigated, the spreading of the two-dimensional hot jet is not as spectacular as in the axisymmetry case.

1. Introduction

The large-scale structures in the near field of a jet and their relation to hydrodynamic instability have been investigated extensively for a number of reasons: one is their role in laminar–turbulent transition, another is the potential of stability–theoretical models for flow control aimed at better mixing for instance. The behaviour of inhomogeneous jets in particular has been a subject of considerable research in recent years. It has in part been motivated by the study of Monkewitz & Sohn (1986, 1988) who showed that a hot axisymmetric gas jet can develop a region of local absolute instability in the potential core region if the jet density is less than 0.72 times the ambient density. This result suggested that lowering the jet density may lead to self-excited oscillations or global instability of the jet. Such oscillations, associated with line-dominated power spectra were indeed discovered experimentally in a round helium–air jet by Sreenivasan, Raghu & Kyle (1989) and Kyle & Sreenivasan (1989) and in a heated air jet by Monkewitz *et al.* (1989, 1990) and Raghu & Monkewitz (1991). All the experiments showed that the oscillatory behaviour is intrinsic to low-density jets and insensitive to small perturbations, much like Kármán vortex shedding is intrinsic to the cylinder wake. At the same time, Monkewitz *et al.* (1989, 1990) found that self-excited oscillations were associated with a dramatic jet spreading.

† Current address: Mechanical Engineering Department, National Sun Yat-Sen University, Kaohsiung, Taiwan 80424.
‡ Current address: Department of Mechanics, ME-Ecublens, Federal Institute of Technology, CH-1015 Lausanne, Switzerland.

The nature of oscillations in low-density non-circular jets, on the other hand, has not been investigated. This has motivated the present experimental effort aimed at a better understanding of the effect of jet density on the global behaviour of a two-dimensional hot jet in which the initial mixing layers are laminar and buoyancy effects are negligible in the near field. For this study the Mach number is near zero, and the Reynolds number is around 4000, based on the jet width H, the jet-exit velocity u_j and viscosity at the ambient temperature T_∞. The dominant parameter governing the nature of the jet instability is the ratio of the jet-exit to ambient density, in short called density ratio and denoted by S. The main question we are addressing is whether, and under what conditions, the two-dimensional hot jet exhibits self-excited oscillations.

Based on linear stability analysis, Yu & Monkewitz (1990) showed that a two-dimensional jet contains regions of absolute instability where the ratio of the jet centreline to ambient density is below 0.95. According to the recent analysis of global modes by Chomaz, Huerre & Redekopp (1991) and Monkewitz, Huerre & Chomaz (1993), two-dimensional jets with $S < 0.95$ have the potential for global instability. With this in mind, a jet facility was built to produce a two-dimensional air jet in which the density ratio could be varied between 0.73 and unity by heating the jet. The experimental facility is described in §2.

The experimental results are presented in §3. First, we document the quality of the jet facility in terms of the mean flow variations in the potential core region with and without jet heating. Secondly by using spectral and bicoherence measurements of velocity and temperature, we demonstrate that self-excited oscillations occur in the two-dimensional hot jet at density ratios below approximately 0.9, which is significantly higher than the critical value of around 0.7 previously found in round jets (Monkewitz *et al.* 1990). Finally, the spreading of the self-excited two-dimensional hot jet is explored with flow visualization and compared to that of the round jet.

2. The experimental apparatus

2.1. *Facility*

The facility used to produce a two-dimensional hot jet with an aspect ratio of 20:1 is shown on figure 1. A variable-speed blower delivers air to the jet through a long duct and an acoustic muffler lined with fibreglass to reduce blower noise. The air then passes through a 6.5 kW electric heater packed with aluminium wool, which makes the velocity and temperature distributions uniform. A two-dimensional divergent–convergent settling chamber is acoustically lined with 1 in. thick fibreglass, and a layer of steel wool is installed at the largest cross-section of the chamber to reduce large-scale turbulence and further smooth the temperature distribution. A layer of honeycomb and several screens provide the final turbulence management before the 10:1 contraction. This last part of the flow facility after the screens has a smooth Formica inner surface and is thermally insulated with fibreglass on the outside. The nozzle measures 15×300 mm and points vertically up. As shown on figure 1, x, y and z denote the streamwise, cross-stream and spanwise coordinates, respectively, normalized by the jet width $H = 15$ mm. Plexiglas plates are attached to both sides of the nozzle, parallel to the (x, y)-plane, to prevent the jet spreading in the z-direction, thus improving the two-dimensionality of the jet.

The facility was required to be as quiet as possible during the experiments. In addition to the use of fibreglass in the settling chamber and the acoustic muffler, the noise level in the laboratory was minimized by carrying out the experiments at night and switching off all unnecessary equipment during data acquisition. The resulting

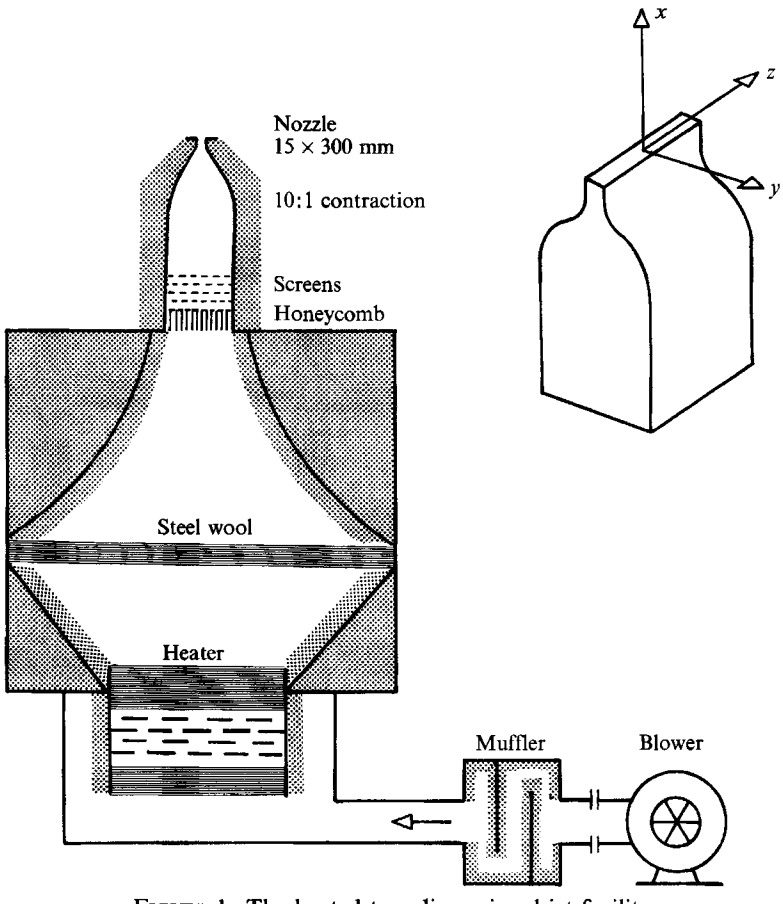

FIGURE 1. The heated two-dimensional jet facility.

r.m.s. turbulence level in the nozzle exit plane of the unheated jet was determined with a constant-temperature hot wire and found to be less than 0.06% for a jet velocity of 4.5 m/s.

Limited by the temperature tolerance of the fabrication material, plywood, the experiments have been carried out with jet temperatures ranging from room temperature, which was always close to 20 °C, to 130 °C. Hence the facility can provide a hot jet with density ratios between 0.73 and unity. At the highest jet temperature and a jet velocity of 4 m/s a Reynolds number of about 4000 can be obtained corresponding to an exit Richardson number, defined as $gH(1-S)[Su_j^2]^{-1}$, of about 3×10^{-3}. Hence buoyancy forces are insignificant in the near field of the hot jet.

2.2. *Instrumentation*

For the experiments the facility was instrumented as follows. The operating parameters, jet-exit temperature and velocity, were obtained by a Chromel–Alumel (K-Type) thermocouple probe with a junction of 2 mm diameter and an MKS pressure transducer (type 398HD) with a total head probe of 1 mm diameter. The thermocouple and Pitot/pressure transducer were also used to calibrate a DANTEC hot-wire anemometer in constant-current and constant-temperature modes for local unsteady temperature and velocity measurements, respectively. The hot-wire probe (DANTEC type 55 P11) had a 5 μm platinum-plated tungsten wire with a working length of

1.25 mm. The frequency response in constant-current mode was tested by heating the wire sensor with a laser beam which was switched on and off by an acousto-optical modulator. The time constant was estimated to be 1.8 ms, corresponding to a cut-off frequency $f_{-3dB} \approx 90$ Hz which is adequate for the present experiments.

In constant-temperature mode, an overheat ratio of 0.8 was used for velocity measurements in the homogeneous jet. The mean values of the hot-wire signals, either in constant-current or in constant-temperature modes, were obtained by a DANTEC mean value unit Type 56N22 with integration times up to 1000 s. The fluctuating data were collected by an HP 3400A r.m.s. voltmeter and/or a HP 3582A Spectrum Analyzer. In addition, a MetraByte analog-to-digital converter was used to digitize the hot-wire signals for further data processing. The near-field pressure outside the jet was monitored by a $\frac{1}{2}$ in. B & K microphone fitted with a standard protective cap to shield it from the entrainment flow.

Flow visualization was carried out by two methods. The first was schlieren, using a system with two spherical mirrors of 15 cm diameter and 150 cm focal length. A XENON (Model 437B) 20 ns spark gap served as light source and, to obtain sensitivity to all directions of density gradient, a 2 mm diameter pinhole and an iris were substituted for the usual slit and knife edge (Liepmann & Roshko 1957). The second method to visualize the cross-section of the jet used laser sheet illumination of smoke injected into the jet fluid upstream of the heater. The laser sheet of about 1 mm thickness was obtained by using a cylindrical lens to expand the laser beam of a 5 W Ar–ion laser. In both cases, a Nikon camera with 3200 ASA high-speed film was used to record the flow visualizations.

3. Results and discussion

3.1. *The mean flow data*

The mean velocity and temperature profiles in the nozzle plane have been measured to document the quality of the two-dimensional hot-jet facility. As shown on figure 2, the mean temperature variation between $z = -7$ and $+7$ along the nozzle is less than 3% of the temperature difference between the jet centreline and the ambient, $\Delta T = T_j - T_\infty$, for a jet total head $q_j = 0.79$ mmH_2O as an example. We remind the reader here that throughout the paper, coordinates are non-dimensionalized with the nozzle width H. For quantities other than coordinates, the distinction between their dimensional and non-dimensional form is made wherever necessary by stating the dimension explicitly. The velocity profiles as a function of z are also uniform both at $x = 0$ and $x = 8$, except for thin boundary layers on both ends, as also shown on figure 2. This demonstrates the good two-dimensionality of the jet flow over the central 70% of the nozzle length. In addition, the temperature distributions in the y-direction, i.e. across the nozzle, are symmetric with respect to the centreplane $y = 0$ and are identical within 5% of ΔT at the stations $z = -6.7$, 0 and $+6.7$, as illustrated on figure 3. We note that on this figure the temperature outside the jet is higher than the room temperature of 20 °C. This is because for $|y| > 0.5$ the hot wire is traversed less than 1 mm above the hot nozzle material (see also figure 4*b*). The thermal boundary-layer thickness normalized by the jet width, defined by $\Delta T/(\mathrm{d}\bar{T}/\mathrm{d}y)_{max}$, is about 0.14 at $x = 0$ and a jet total head of 0.75 mmH_2O.

The streamwise development of mean profiles is shown in the following. The mean temperature profiles $\bar{T}(y)$ were determined with a constant-current hot wire. They are shown in figures 4(*a*) and 4(*b*) for the slightly heated jet with $S = 0.95$ and the hot jet with the same total head of 0.75 mmH_2O and $S = 0.76$, respectively. The profiles $\bar{T}(y)$

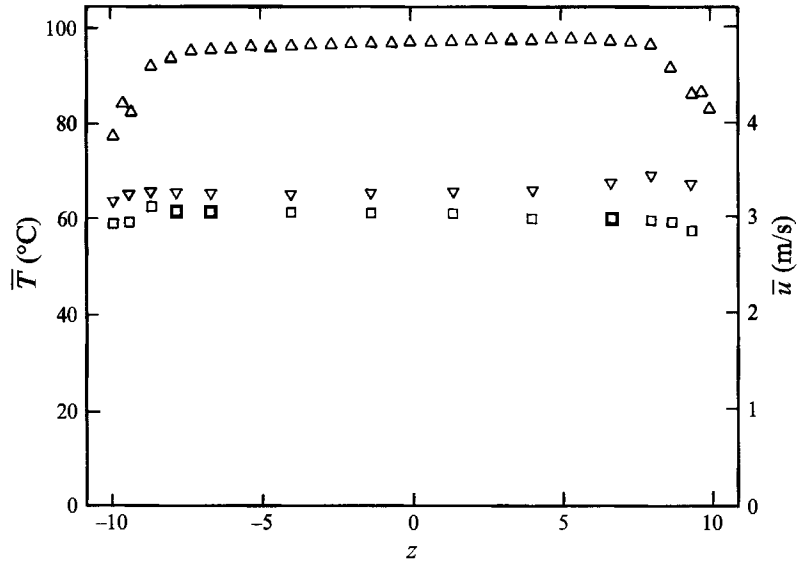

FIGURE 2. Mean temperature profile $\bar{T}(z)$ at $x = y = 0$ (△) for $q_j = 0.79$ mmH$_2$O. Mean velocity profiles $\bar{u}(z)$ at $y = 0$, and $x = 0$ (▽), $x = 8$ (□) for $S = 1$.

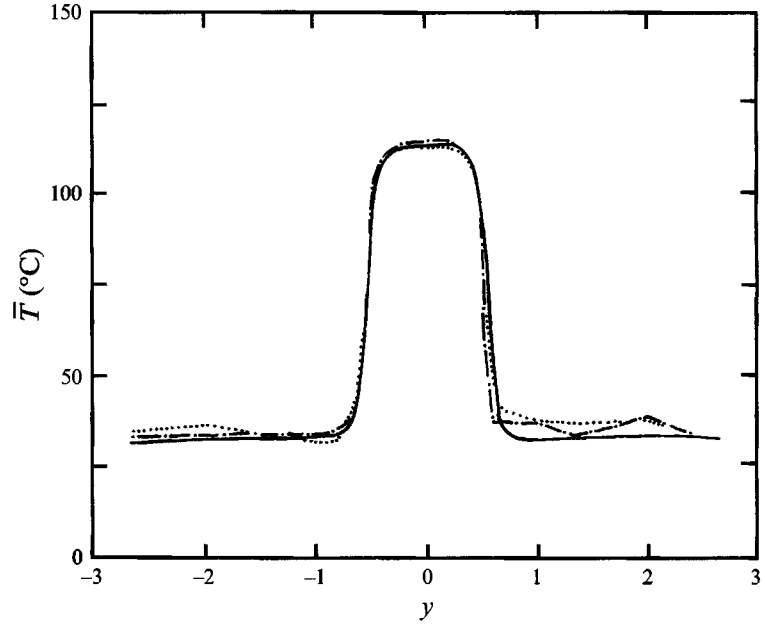

FIGURE 3. $\bar{T}(y)$ at $x = 0$, and $z = -6.7$ (· · · ·), $z = 0$ (——), $z = 6.7$ (—·—), for $q_j = 0.75$ mmH$_2$O.

are very similar in both cases except at $x = 6$, where the hot jet shows a faster decay of centreline temperature and more spreading. For $x = 4, 6$ of figure 4(*b*), intermediate plateau appear in the shear layers, which coincide with the location of the cores of the highly organized large vortex-pair structures seen in the flow visualization of §3.4 below.

In order to determine transverse mean velocity profiles in the hot jet, total-head profiles $\bar{q}(y)$, shown in figure 5 again for $q_j = 0.75$ mmH$_2$O, have been used in

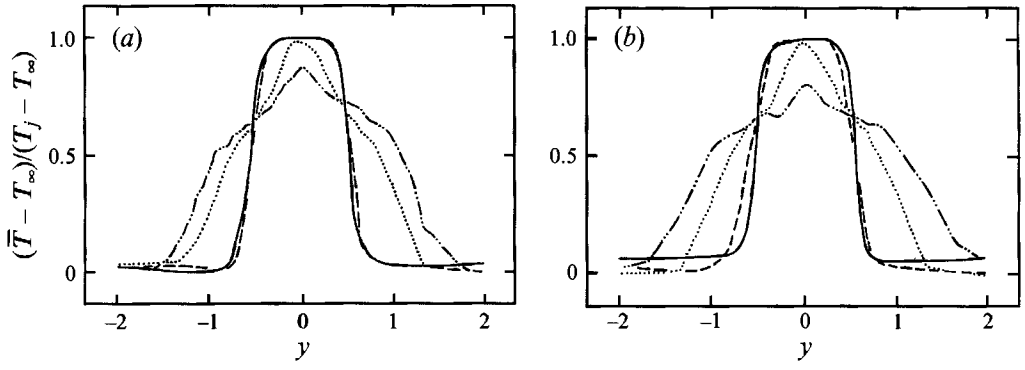

FIGURE 4. Mean temperature profiles of the heated jet for $q_j = 0.75$ mmH$_2$O, at $x = 0$ (——), 2 (– – –), 4 (· · · · · ·), 6 (— · · —): (*a*) $S = 0.95$, (*b*) $S = 0.76$.

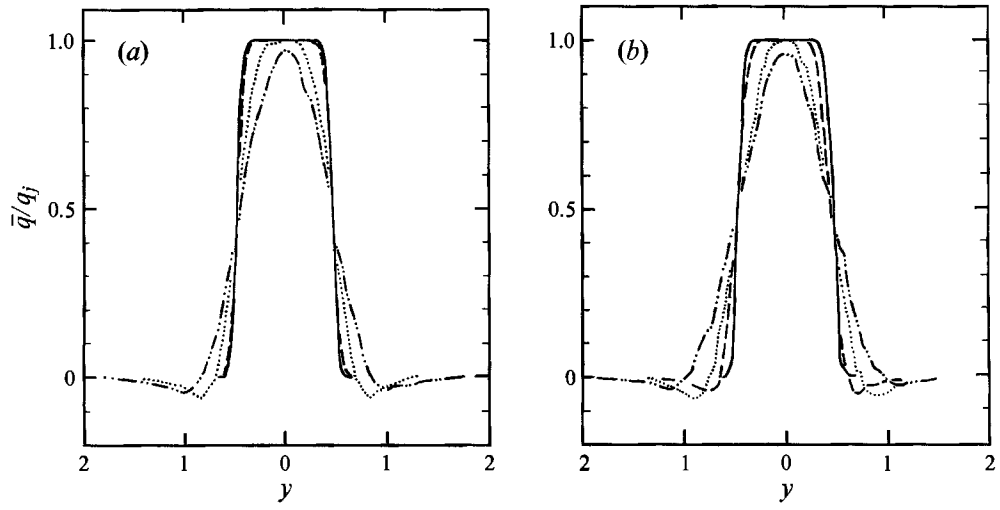

FIGURE 5. Mean total-head profiles of (*a*) the homogeneous jet ($S = 1$) and (*b*) the heated jet with $S = 0.76$, for $q_j = 0.75$ mmH$_2$O, at $x = 0, 2, 4, 6$ (curves as in figure 4).

conjunction with the mean temperature data of figure 4. To allow an unbiased comparison with the cold jet, the total-head profiles for $S = 1$ are included as figure 5(*a*). From this, the transverse mean velocity profiles at different downstream stations are obtained. The velocity profiles for the cold jet derived from the total-head profiles of figure 5(*a*) are shown on figure 6(*a*). Comparing figure 6(*a*) with the constant-temperature hot-wire measurements of figure 6(*b*) shows that while the central portion of the profiles are essentially identical, the total-head probe yields unacceptable results in the regions of low velocity, in particular at $x = 4$ and 6. The reasons for this are the poor sensitivity of the probe at low speed and, more importantly, the below-ambient static pressure just outside the jet, which drives the entrainment flow (see figures 5*a* and 5*b*).

Figure 6(*b*) for the cold jet in particular illustrates well the symmetry during the flow development. In addition, it allows an estimate of the non-dimensional momentum thickness θ/H, defined for the cold jet by

$$\frac{\theta}{H} = \int_0^\infty \frac{\bar{u}}{u_j}\left(1 - \frac{\bar{u}}{u_j}\right) \mathrm{d}y.$$

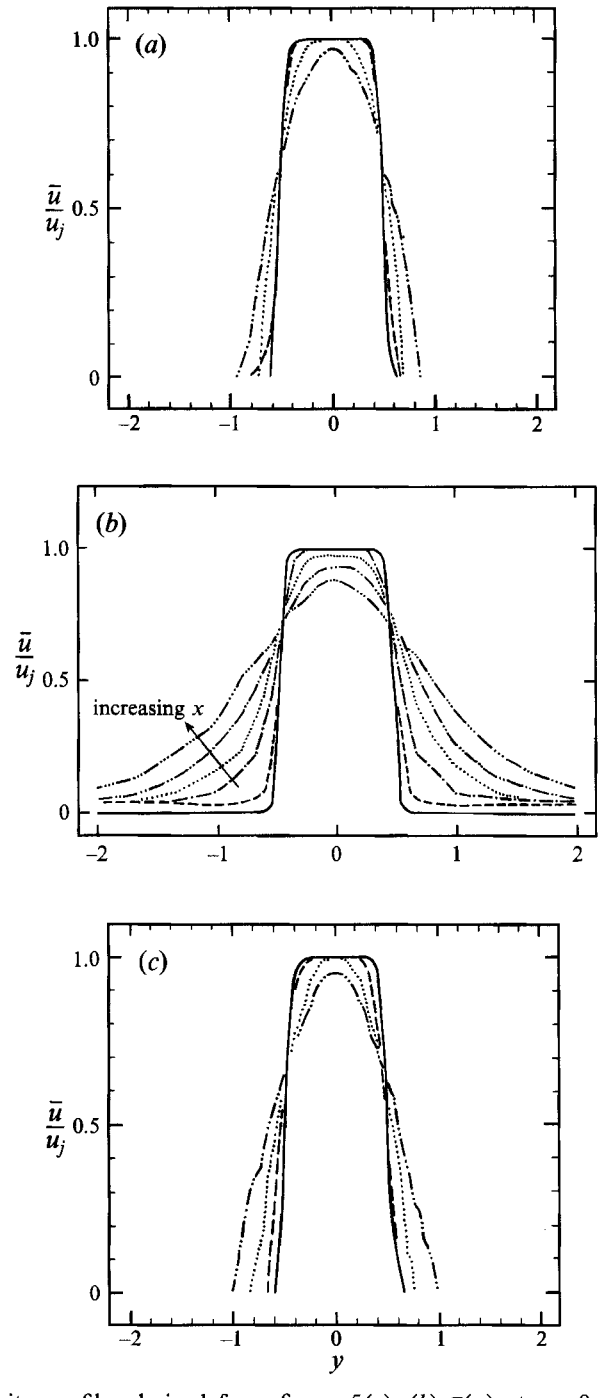

FIGURE 6. (*a*) Velocity profiles derived from figure 5(*a*). (*b*) $\bar{u}(y)$ at $z = 0$, $x = 0, 2, 3, 4, 6, 8$ for $q_j = 0.75\,\mathrm{mmH_2O}$, $S = 1$. (*c*) Velocity profiles derived from figure 5(*b*) and corresponding temperature profiles of figure 4(*b*).

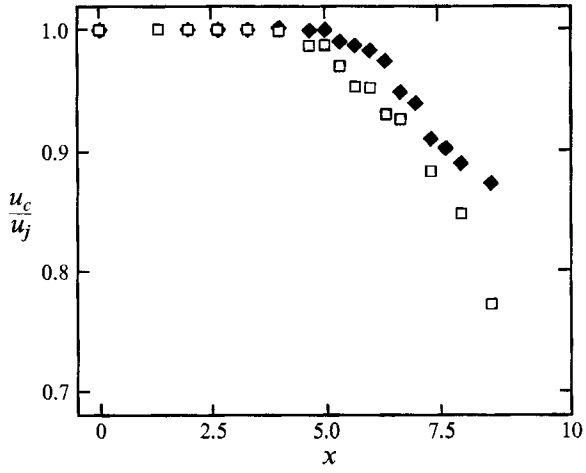

FIGURE 7. Centreline velocity versus x for $S = 1$ (◆) and $S = 0.76$ (□) at $Re = 4000$.

For $S = 1$ it was measured to be $\theta/H = 1.14\,Re^{-\frac{1}{4}}$ at $x = 0$, which demonstrates laminar initial conditions. The non-dimensional vorticity thickness, defined as $\delta_\omega/H = \Delta u/(\mathrm{d}\bar{u}/\mathrm{d}y)_{max}$, is 0.15 at $x = 0$ and a jet total head of 0.75 mmH_2O. Comparison with figure 3 shows that the thickness of the velocity and thermal boundary layers at the jet exit are approximately equal at equal total heads (note that, owing to the temperature difference, the Reynolds number in figure 6*b* is 13% lower than in figure 3).

The mean velocity profiles derived from total-head measurements in the hot jet with $S = 0.76$ are shown on figure 6(*c*). It appears from the velocity profile at $x = 6$ in particular, that at the end of the potential core the hot jet spreads somewhat faster than the cold jet. This is supported by the streamwise development of the centreline velocities on figure 7, which shows an earlier decay for the hot jet than for a cold jet of equal Reynolds number. Further aspects of spreading and mixing will be discussed in §3.4.

3.2. *Amplitude spectra*

Three kinds of fluctuating data – temperature, velocity, and pressure – are analysed in the frequency domain to illuminate the jet behaviour. The pressure signals turned out to have the poorest signal-to-noise ratio. The microphone was therefore only used to monitor the noise associated with the building ventilation system in order to stay away from its spectral peaks at 60 and 120 Hz. Since the hot wire in constant-temperature mode is sensitive to both velocity and temperature fluctuations, the acquisition of velocity signals in the hot jet is restricted to the entrainment region where the temperature is constant and equal to the ambient. In the shear layers of the hot jet the temperature and velocity fluctuations are comparable and the hot wire was therefore operated in constant-current mode so as to sense only temperature.

3.2.1. *Line-dominated spectra*

The near-field velocity spectra of the cold and hot jet shown on figure 8 were obtained with the hot-wire probe inserted in the entrainment region outside but close to the shear layers (see for instance the hot-wire probe location in figure 18*a*). As demonstrated by these velocity spectra, a cold jet has broadband spectra while the hot-jet spectra are line-dominated with a substantial harmonic content, which suggests a behaviour as a nonlinear oscillator. The temperature spectra in the shear layer are shown on figure 9 for increasing jet temperature and the two transverse positions where the spectral components at $f_0 \approx 50$ Hz and $2f_0$, respectively, peak. Figure 9

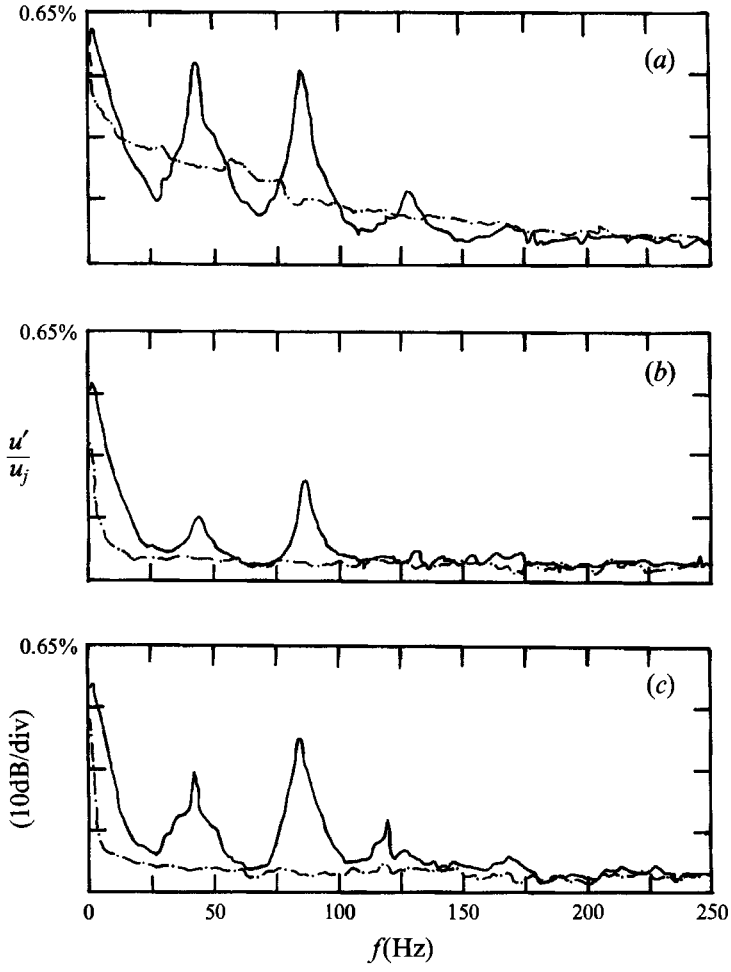

FIGURE 8. Velocity spectra of the cold jet $S = 1$ (—·—) and the hot jet with $S = 0.76$ (——) at different locations in the entrainment region for $q_j = 0.85$ mmH$_2$O: (*a*) at $x = 2.00$, $y = 1.33$; (*b*) $x = 1.00$, $y = 1.00$; (*c*) $x = 1.00$, $y = 0.67$.

demonstrates that the transition from the broadband spectrum of a slightly heated jet to the line-dominated spectrum of hot jets takes place at $S \approx 0.9$. The spectra for $S < 0.9$ are reminiscent of cylinder wakes where they have been shown to correspond to limit-cycle oscillations. However, in contrast to the wake the hot-jet oscillation is dominated by the varicose mode as expected from linear stability (Yu & Monkewitz 1990) and confirmed by flow visualization in §3.4.

In the hot jet at $S = 0.75$ where the spectra are line-dominated, the evolution of instability waves in the streamwise direction, as characterized by the amplitudes of the spectral lines f_0 and $2f_0$ were examined as follows. First, the maximum amplitudes with respect to the y-direction at a fixed streamwise location were obtained for the dominant lines f_0 and $2f_0$ which correspond to Strouhal numbers $St = fH/u_j$ of 0.16 and 0.32 respectively. These maximum amplitudes versus the streamwise coordinate are shown on figure 10(*a*). The corresponding y-locations of the largest f_0- and $2f_0$-peaks are documented in figure 10(*b*), which shows that the largest temperature fluctuations at the lower frequency f_0 are found further away from the centreline than the largest fluctuations at $2f_0$.

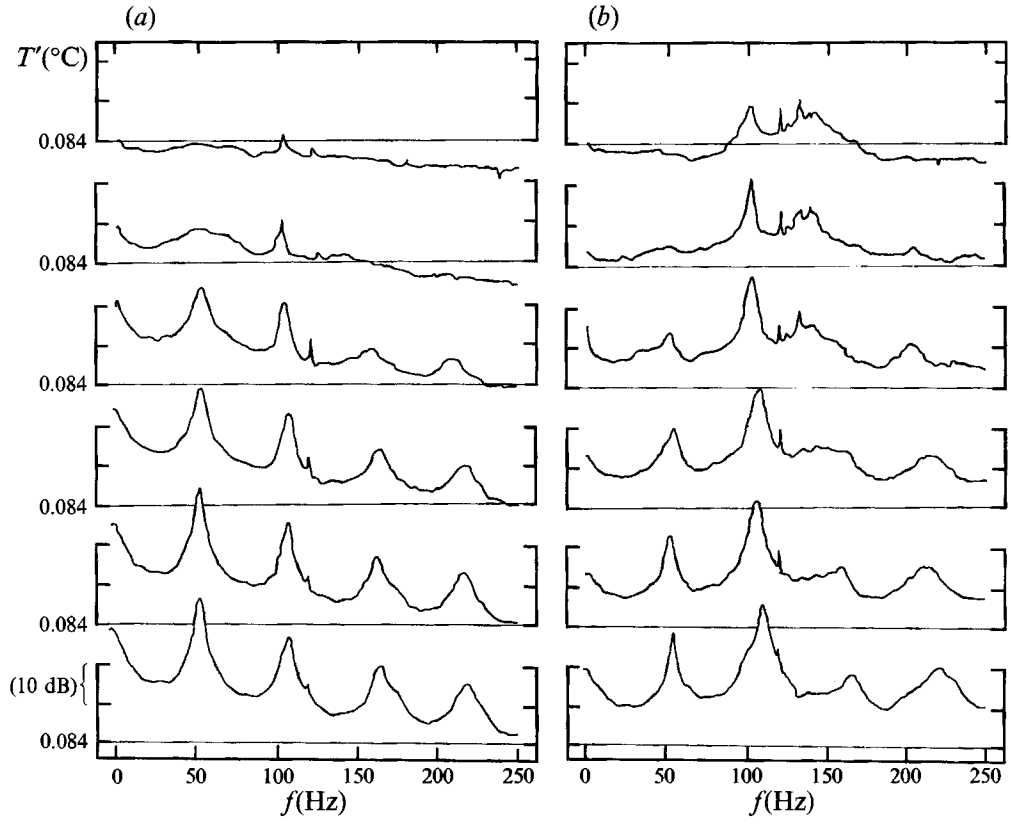

FIGURE 9. Temperature spectra as function of density ratio for constant total head $q_j = 1.26$ mmH$_2$O, hot-wire probe at $x = 3$ and y-locations where either the f_0 or $2f_0$ spectral peak is maximum. (*a*) At maximum amplitude of the first peak (frequency $f_0 \approx 54$ Hz). The spectra were obtained at approximately $y = 0.9$ for each case. From top to bottom $S = 0.97, 0.94, 0.88, 0.85, 0.82, 0.75$. (*b*) At maximum amplitude of the second peak with frequency $2f_0$. The spectra were obtained at approximately $y = 0.4$ for each case. From top to bottom $S = 0.97, 0.94, 0.89, 0.85, 0.82, 0.75$.

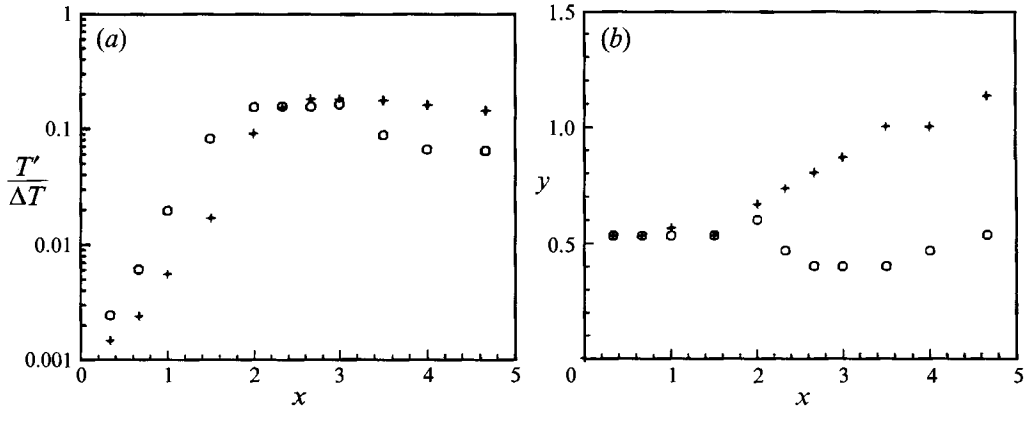

FIGURE 10. (*a*) The maximum temperature amplitude with respect to y versus x for the f_0-peak (+) and for the $2f_0$-peak (○) in the line-dominated spectra, at $q_j = 1.25$ mmH$_2$O and $S = 0.75$. (*b*) The y-location corresponding to where (*a*) was obtained.

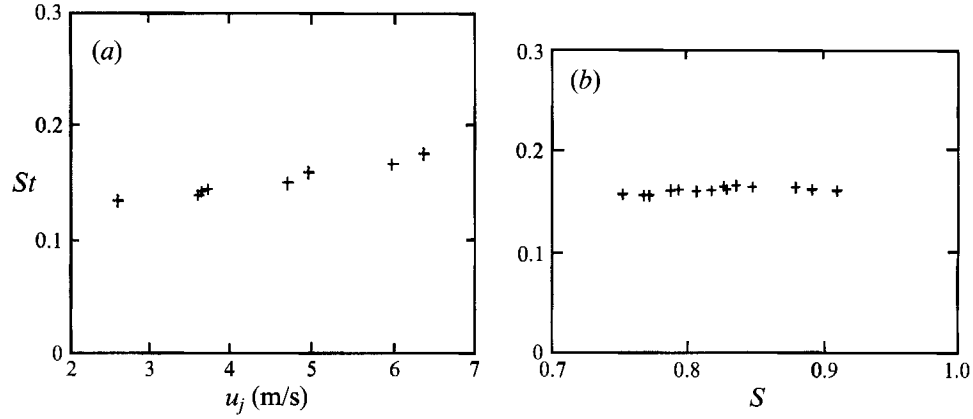

FIGURE 11. (*a*) Strouhal numbers in the line-dominated spectra versus jet velocity for the spectral peak at f_0 and $S = 0.76$. (*b*) Strouhal number versus density ratio at $q_j = 1.26$ mmH_2O, $x = 3$ and y where the maximum amplitudes were obtained for the peak at f_0 in the line-dominated spectra.

First one notes that on figure 10(*a*) the amplitude of both frequency components increases approximately exponentially with x in the region $x \lesssim 1.4$ close to the nozzle. We emphasize that this does not allow the conclusion that the jet oscillations are just spatially amplified disturbances introduced at the nozzle. As shown in the next section, the exponential 'tails' near the nozzle should, rather, be interpreted as part of a global mode (Huerre & Monkewitz 1990).

The second comment in connection with figure 10(*a*) is that the $2f_0$-peak dominates near the nozzle while the 'subharmonic' f_0 takes over beyond $x \approx 3$. This points to a vortex pairing process between $x = 2$ and 3, which is confirmed by the flow visualization of §3.4. When the jet oscillations are self-excited, this raises the question, to be addressed in the following sections, of whether the frequency of the primary or driving oscillator is that of the 'fundamental' or the 'subharmonic'.

3.2.2. *The dominant Strouhal number*

In homogeneous two-dimensional jets, Ho & Hsiao (1982) found that the vortex passage frequency (measured at the inner edge of the shear layer) is a function of the streamwise distance. From the nozzle to the end of the potential core, the higher frequency of the 'shear-layer mode' drops to the lower frequency of the 'preferred mode' which is only weakly dependent on initial conditions (see also Ho & Huerre 1984). The frequency f_0 in the hot jet is now shown to be close to the frequency of the preferred mode, which means that it does not scale with the local shear-layer thickness. According to Monkewitz & Huerre (1982), for instance, the most amplified spatial shear-layer mode has a frequency of $f\delta_\omega/u_j = 0.07$ leading to $f \propto u_j^{\frac{3}{2}}$ for $\delta_\omega \propto u_j^{-\frac{1}{2}}$. Figure 11(*a*) clearly demonstrates that the observed oscillations in the hot jet cannot be related to shear-layer modes as the frequency f_0 is only weakly dependent on velocity. The trend to lower Strouhal numbers at lower velocity may be qualitatively explained by the increased shear-layer thickness throughout the potential core region, which slightly modifies the global stability properties (see Yu & Monkewitz 1990 for the dependence of absolute frequency on shear-layer thickness).

Furthermore, the frequency f_0 is found to be essentially independent of the density ratio S in all cases with line-dominated spectra, as evidenced by figure 11(*b*). Finally, using the mean flow data of §3.1 at $x = 0$, the Strouhal number of the most amplified initial (spatial) shear-layer mode for $q_j = 1.26$ mmH_2O and $S \approx 0.75$ is estimated to be

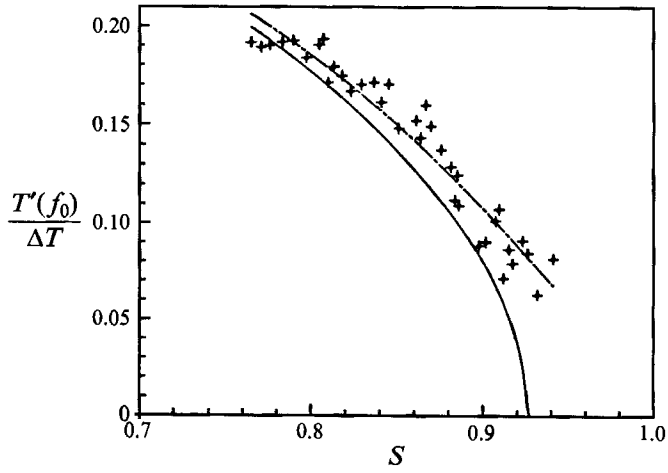

FIGURE 12. Normalized temperature amplitude of the spectral peak at f_0 versus density ratio S for $q_j = 1.26\ \mathrm{mmH_2O}$: —·—, equation (2) fitted to the f_0 data with $S_{crit} = 0.927$, $C_n/C_l = 4.07$, $\alpha_f/C_l = 2.4 \times 10^{-3}$; ——, equation (2) with same S_{crit} and C_n/C_l, but $\alpha_f/C_l = 0$. The hot-wire probe was at $x = 3.0$ and the y-location where the f_0-peak has the maximum amplitude.

$St = fH/u_j \approx 0.6$, significantly higher than the observed value of 0.32 corresponding to the $2f_0$-peak on figure 11(*b*). This value is close to the band of $0.2 \lesssim St \lesssim 0.3$ of computed local Strouhal numbers $St = \omega_r^0/2\pi$ (Yu & Monkewitz 1990) for which the absolute growth rate is positive. We note that the similarity of the saturated limit-cycle frequency and the local absolutely unstable frequencies, computed on a linear basis, has in general no firm theoretical basis. Nevertheless, as in the wake (see for instance Hannemann & Oertel 1989) it supports the notion that the observed strong jet oscillations are related to absolute instability, i.e. to feedback by upstream vorticity waves, in the manner suggested by Huerre & Monkewitz (1990).

3.2.3. *The self-excited nature of the jet oscillations*

The dominant frequencies in an oscillating hot jet, i.e. the frequencies corresponding to the spectral peaks of figure 8, do not vary with location. We also reiterate that they are different from those of the acoustic noise spectrum when the jet is turned off. This supports the hypothesis that the hot-jet oscillations are not the result of ambient noise amplification. Furthermore, the weak frequency variation with S of figure 11(*b*) eliminates the possibility of acoustic cavity resonances in the settling chamber. In the following, we produce more direct evidence to show that the spectra for $S \lesssim 0.9$ indeed correspond to a stable nonlinear saturation state, i.e. a limit cycle.

As already shown on figure 9, the broadband spectra become line-dominated with decreasing density ratio. When the normalized peak amplitude of the spectral line f_0 of figure 9(*a*) is plotted as a function of density ratio, a Hopf bifurcation diagram is found as illustrated in figure 12. The similarities to the global behaviour of the cylinder wake, as investigated by Provansal, Mathis & Boyer (1987) and others, are immediately apparent. As in the cylinder case, the characteristic amplitude of the oscillation (say, the amplitude at any fixed location) is found to be described by a Landau equation in the neighbourhood of the bifurcation:

$$\frac{\mathrm{d}|A|}{\mathrm{d}t} = \sigma|A| - C_n|A|^3 + \alpha_f. \tag{1}$$

In (1) a forcing term has been added to account for external forcing by noise, which

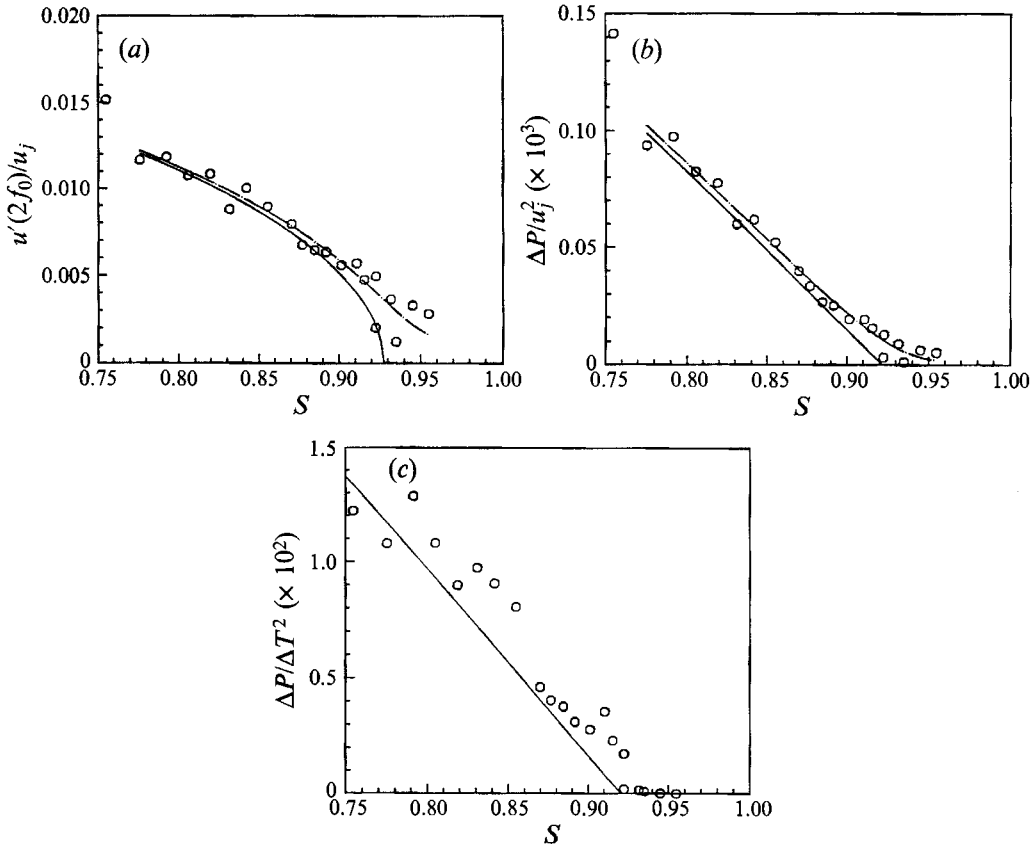

FIGURE 13. (*a*) Normalized velocity amplitude of the spectral peak at $2f_0$ versus density ratio S for $q_j = 1.26$ mmH_2O: —·—, equation (2) fitted to the $2f_0$ data with $S_{crit} = 0.927$, $C_n/C_l = 1.046 \times 10^3$, $\alpha_f/C_l = 4.926 \times 10^{-5}$. ——, equation (2) with same S_{crit} and C_n/C_l, but $\alpha_f/C_l = 0$. The hot-wire probe was at $x = 1.5$ and a y-location in the entrainment region outside but close to the shear layers. (*b*) Normalized ΔP, defined in equation (3) with $\Delta f = 1.94$ Hz, of velocity versus S at nominally same conditions as in (*a*). (*c*) Normalized ΔP of temperature versus S for $q_j = 1.26$ mmH_2O. The hot-wire probe was at $x = 1.5$ and the y-location where the $2f_0$-peak has maximum amplitude.

is always present in an experiment. The temporal growth rate σ in (1) is to leading order proportional to $(S_{crit} - S)$, i.e. $\sigma = C_l(S_{crit} - S)$. For $C_n > 0$, the cubic nonlinearity limits the amplitude, and the saturated limit-cycle amplitude, $|A|_{sat}$, is obtained from (1) by setting $\mathrm{d}|A|/\mathrm{d}t = 0$:

$$(S_{crit} - S)|A|_{sat} - (C_n/C_l)|A|_{sat}^3 + (\alpha_f/C_l) = 0. \tag{2}$$

For zero noise $\alpha_f = 0$, the solution is $|A|_{sat}^2 = (C_l/C_n)(S_{crit} - S)$. For the amplitude of the $2f_0$ spectral component, the entrainment velocity at $x = 1.5$ shown on figure 13(*a*) turned out to provide the most reliable global measure, while temperature fluctuations in the thin shear layer at $x = 1.5$ are strongly affected by any low-frequency lateral motion of the jet induced by draughts in the laboratory, for instance. To improve the confidence in the estimate of $S_{crit} \approx 0.93$ from figure 13(*a*), the data have been reprocessed by integrating the power spectral density PSD(f) over a frequency interval $2\Delta f$ centred on $2f_0$:

$$\Delta P = \int_{2f_0 - \Delta f}^{2f_0 + \Delta f} \mathrm{PSD}(f)\,\mathrm{d}f. \tag{3}$$

The result with the fit $|A|^2_{sat}$ from (2) is shown on figure 13(*b*) and yields $S_{crit} = 0.92$, in close agreement with the value obtained from peak amplitudes. For comparison, the integrated PSD of the temperature fluctuations in the shear layer, normalized by the total temperature difference $\Delta T = T_j - T_\infty$, are shown on figure 13(*c*). Despite the larger scatter due to low-frequency noise and the larger uncertainty for small ΔT, the data are consistent with the bifurcation deduced from the entrainment velocity. It is therefore concluded that the observed oscillations become self-excited via a supercritical Hopf bifurcation (Drazin & Reid 1981, Chap. 7) at approximately $S = 0.92 \pm 0.02$. At this point the question has to be asked what the role of the spectral peak at f_0 is. The amplitude of the f_0 spectral peak of figure 12 was obtained at $x = 3$ where the f_0-component is dominant. At this location the shear-layer thickness is such that the sensitivity of the temperature to low-frequency disturbances is greatly reduced, while the entrainment velocity becomes noisy in turn. It is seen that the analysis of both the f_0- and $2f_0$-components yields the same critical density ratio within the estimated uncertainty of ± 0.02. We therefore suggest that the spatial structure of the limit-cycle oscillations under investigation results from a 'fundamental' global mode at $2f_0$ phase-locked with its 'subharmonic' at f_0. Furthermore, we submit that $2f_0$ represents the primary oscillator or 'driver' frequency. This conclusion is based on the comparison of Strouhal numbers with the unstable absolute frequencies computed by Yu & Monkewitz (1990) and on the fact that near the nozzle the $2f_0$-component dominates and therefore cannot just be the result of a self-interaction of the f_0-component. To further strengthen the evidence, it will be shown in §3.3 that the frequency components at f_0 and nf_0 are phase-locked when $S < S_{crit}$.

3.3. *Investigation of nonlinear interactions by bicoherence analysis*

The amplitude spectrum has been used to analyse the frequency content of the velocity and temperature fluctuations in a hot jet. However, the amplitude spectrum cannot provide information about nonlinear interactions among the spectral components. For this, the bispectrum or its normalized form, the bicoherence spectrum, must be considered. Among others, Knisely & Rockwell (1982) used bicoherence analysis to study flow nonlinearity in an impinging shear layer. Miksad *et al.* (1982) and Miksad, Jones & Powers (1983) investigated the nonlinear interactions in a laminar two-dimensional wake during transition to turbulence by bicoherence spectral measurements.

To define bicoherence, it is necessary to recall the definition of the bispectrum. For any two frequencies f_k and f_l the bispectrum is defined as (Kim & Powers 1979)

$$B(f_k, f_l) = E[X_k X_l \tilde{X}_{k+l}]. \tag{4}$$

Here X_k is the Fourier amplitude at the frequency f_k, $E[\,]$ is the expected value and the tilde denotes the complex conjugate. Physically, the bispectrum measures the production of a third wave with frequency f_m through the (nonlinear) interaction of the primary waves at f_k and f_l. The resulting frequency must thereby satisfy the condition $f_m = f_k + f_l$. The bicoherence spectrum is a normalized version of the bispectrum and is defined as

$$b^2(f_k, f_l) = \frac{|B(f_k, f_l)|^2}{E[|X_k X_l|^2]\, E[|X_{k+l}|^2]}, \tag{5}$$

where $|\,|$ denotes the modulus. The bicoherence spectrum is bounded by $0 \leqslant b^2(f_k, f_l) \leqslant 1$. If the three spectral components at frequencies f_k, f_l and f_m are perfectly phase locked, the bicoherence $b(f_k, f_l)$ is unity. If the phases of the three spectral components are independent of one another, $b(f_k, f_l)$ is zero.

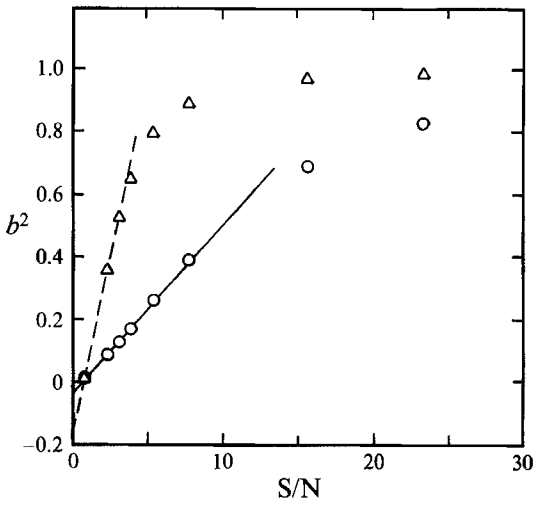

FIGURE 14. $b^2(f_0,f_0)$ (△), $b^2(f_0,2f_0)$ (○) versus S/N ratio for signal given by equation (6), where $S/N = A_1/A_n$. The linear fits included in the plot are good for $0 \lesssim b^2 \lesssim 0.6$.

For bicoherence evaluation, the analog temperature signal from the DANTEC hot-wire anemometer in constant-current mode was processed digitally. After being fed through a low-pass filter with 250 Hz cutoff frequency, the analog signal was amplified and sampled with a 12-bit analog-to-digital converter at a sampling rate of 600 samples per second, and recorded on an IBM PC-AT compatible. Each record contained 80 consecutive blocks of 1024 temperature samples corresponding to 136.53 seconds of real time. To estimate bicoherence, each block was fast-Fourier transformed with $\Delta f = 0.586$ Hz resolution (Oppenheim & Schafer 1975). It is noted that, owing to the symmetry of the bicoherence $b^2(f_k,f_l) = b^2(f_l,f_k)$ and the relation $X_{-m} = \tilde{X}_m$ between Fourier amplitudes, it is sufficient to compute the bicoherence over a triangular domain given by $0 \leqslant f_k \leqslant \frac{1}{2}f_N$ and $f_k \leqslant f_l \leqslant f_N - f_k$ in the (f_l,f_k)-plane, where f_N is the Nyquist frequency (300 Hz in our case). Since we are only interested in the bicoherence of the frequency f_0 of the first spectral peak with other frequencies, only $b^2(f_0,f)$ needs to be calculated.

To test the bicoherence estimator described above, a synthetic signal

$$X(t) = A_1\cos(2\pi f_0 t+\theta)+A_2\cos(4\pi f_0 t+2\theta)+A_3\cos(6\pi f_0 t+3\theta)+A_n n(t) \quad (6)$$

was generated. The amplitudes A_1, $A_2 = 0.84A_1$ and $A_3 = 0.1A_1$ were chosen to be close to the peak amplitudes found in the hot-jet spectrum of figure 9(*a*), the amplitude A_n of the unit white noise $n(t)$ was varied and the phase θ was a random function of time.

The effect of signal-to-noise (S/N) ratio, defined as $S/N = A_1/A_n$, on the bicoherence estimates is shown on figure 14. While the peaks of the amplitude spectrum are still well above the noise, $b^2(f_0,f_0)$ and $b^2(f_0,2f_0)$ degrade rapidly below S/N of about 10. This property is exploited in the following to obtain an estimate of the critical density ratio, which is less affected by external noise.

Evidence has been presented in §3.2 that a hot jet behaves like a nonlinear oscillator with primary frequency $2f_0$ when $S < S_{crit}$. We now show that the $2f_0$-component is phase-locked with its subharmonic at f_0.

The bicoherence of the frequency f_0 with other frequencies has been measured at cross-stream locations where the amplitude of the f_0-component is maximum. For the self-excited hot jet with $S = 0.77$ it is found to be zero except for sharp peaks at

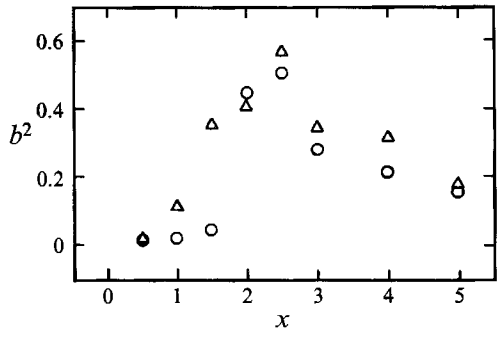

FIGURE 15. Bicoherence $b^2(f_0,f_0)$ (△), and $b^2(f_0,2f_0)$ (○) versus the streamwise location in the hot jet with $S = 0.77$ and $q_j = 1.26$ mmH$_2$O.

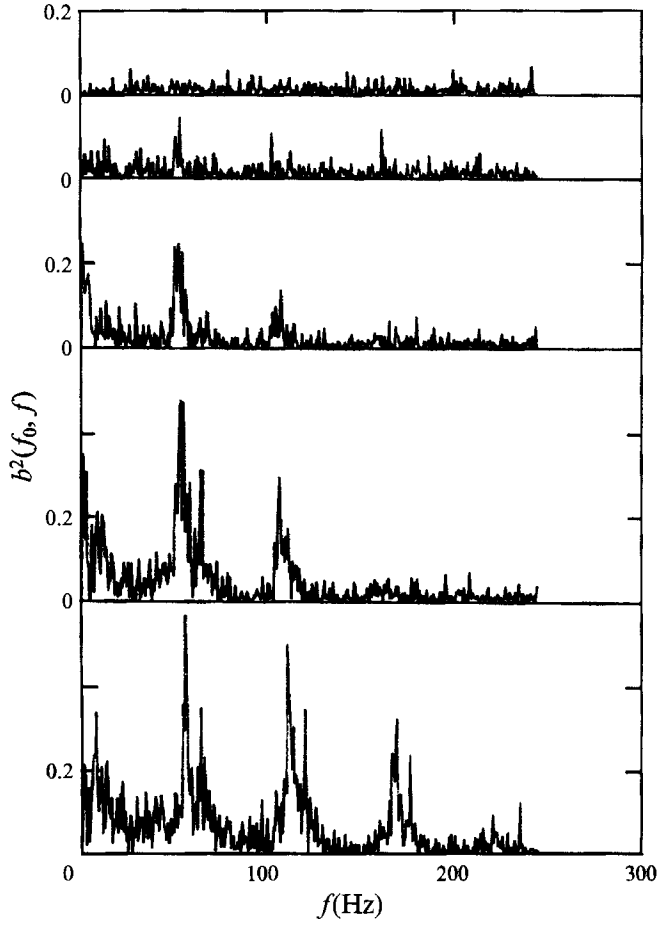

FIGURE 16. $b^2(f_0,f)$ of temperature at $x = 2.5$ and $y = 0.87$ for $q_j = 1.26$ mmH$_2$O and, from bottom to top, $S = 0.77$, 0.86, 0.87, 0.89 ad 0.92.

multiples of f_0. The streamwise evolution of the peaks $b^2(f_0,f_0)$ and $b^2(f_0,2f_0)$ is shown on figure 15. It is seen that these primary bicoherence peaks are not seen for x smaller than approximately 1.5, indicating that the S/N ratio for temperature oscillations in the shear layer close to the nozzle is equal or below unity. Beyond $x = 1.5$, the values

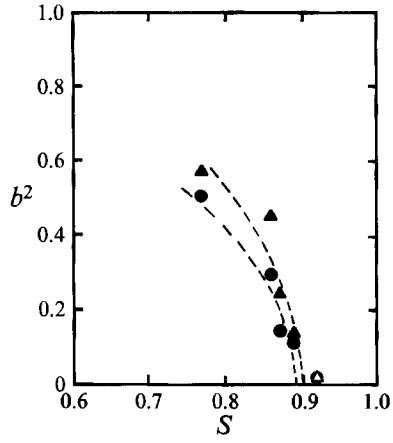

FIGURE 17. Bicoherence $b^2(f_0,f_0)$ (▲), $b^2(f_0,2f_0)$ (●), at $x = 2.5$ and $y = 0.87$, versus density ratio S. ---, relation (8) fitted through the solid symbols.

of $b^2(f_0,f_0)$ and $b^2(f_0,2f_0)$ between 0.3 and 0.6 clearly indicate the nonlinear phase-lock between f_0 and $2f_0$, peaking around $x = 2.5$, the same location where the amplitudes of the f_0- and $2f_0$-components peak on figure 10(*a*) and the first strong vortex pair forms on flow visualizations in §3.4.

To examine the density effect on the nonlinear interaction, the bicoherence spectra of hot jets with varying density ratios were measured at $x = 2.5$ where the maximum bicoherence was obtained (see figure 15). As illustrated on figure 16, with density ratio decreasing, $b^2(f_0,f_0)$ emerges first, then $b^2(f_0,2f_0)$ appears, and finally $b^2(f_0,3f_0)$ also shows up. In other words, more and more of the harmonics of the nonlinear oscillator with the frequency f_0 rise sufficiently above the noise to produce a significant bicoherence as S decreases. We note that for $S = 0.92$ the bicoherence is uniformly close to zero and no clear spectral peaks exist. Under these conditions f_0 was taken to be the same as in the $S = 0.89$ case.

When the $b^2(f_0,f_0)$ and $b^2(f_0,2f_0)$ bicoherence peaks are plotted versus density ratio S on figure 17, a bifurcation diagram very similar to figure 13(*a*) emerges, except that the bicoherence drops to zero at $S \approx 0.9$ much more abruptly than the amplitudes of figures 12 and 13(*a*). The explanation lies in figure 14 which shows that the bicoherence b^2 remains essentially zero when the S/N ratio is increased from zero up to an S/N ratio of order unity, and rises roughly linearly with S/N until it reaches values of 0.5–0.6. In this region one may therefore approximate

$$b^2(f_0,nf_0) - b_n^2 \propto \mathrm{S/N}, \tag{7}$$

where the b_n^2 are the y-intercepts on figure 14 ($b_1^2 \approx -0.14$ and $b_2^2 \approx -0.04$). Noting that the 'signal' in the S/N ratio is nothing other than the saturation amplitude of the limit cycle given by (2), $b^2(f_0,nf_0)$ is now readily related to $(S_{crit} - S)$ if it is assumed that the noise amplitude is independent of or only weakly dependent on S. Because the bicoherence only 'reacts' to signals significantly larger than the noise, it is thereby sufficient to use (2) for $|A|_{sat}$ with $\alpha_f = 0$ which leads to

$$b^2(f_0,nf_0) - b_n^2 \propto (S_{crit} - S)^{\frac{1}{2}}. \tag{8}$$

This relation has been fitted to the data of figure 17 and yields S_{crit} values of 0.90 and 0.89 for $b^2(f_0,f_0)$ and $b^2(f_0,2f_0)$ respectively. It is our experience that the S_{crit} values

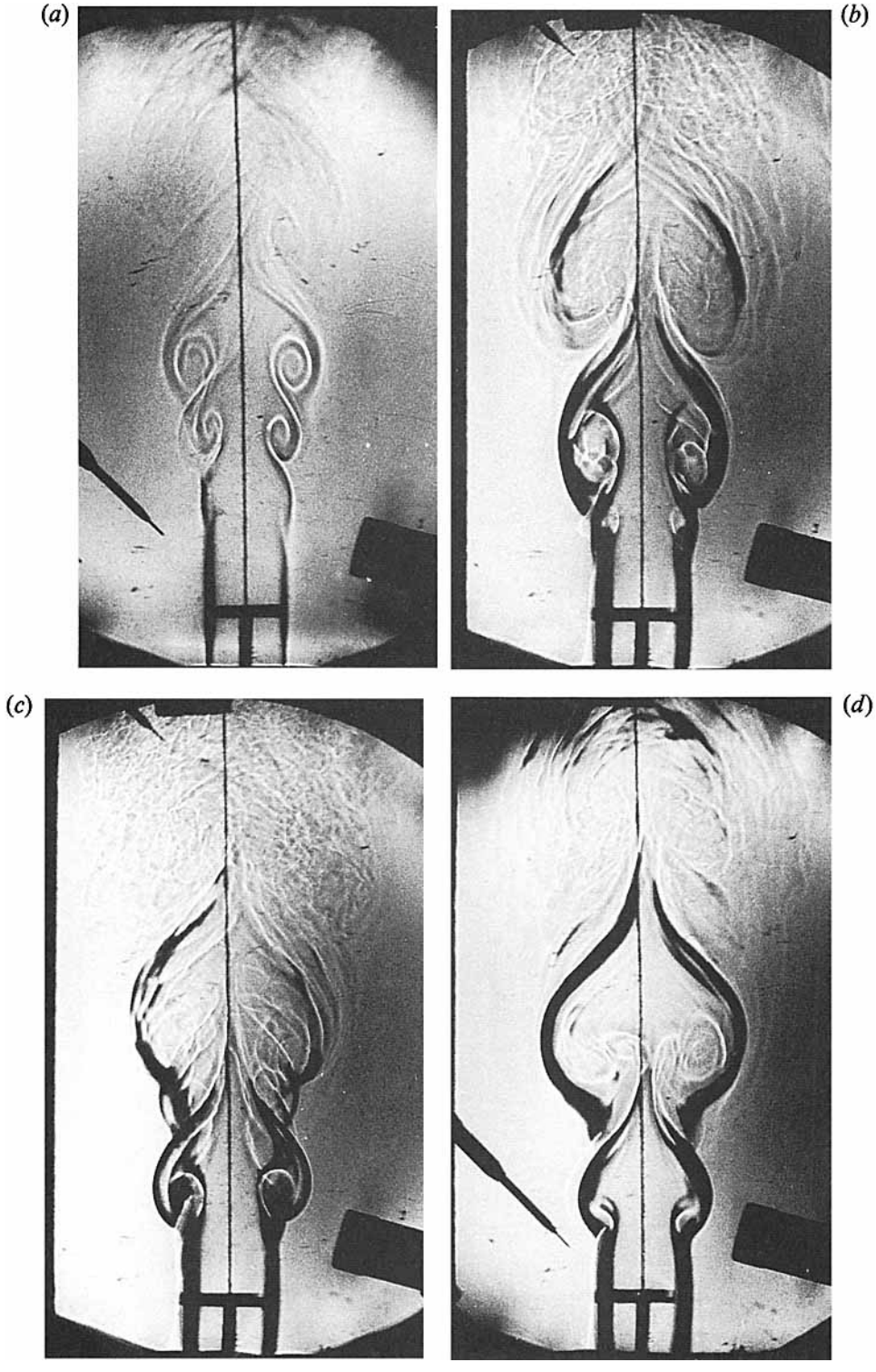

FIGURE 18. Spark schlieren views of the slightly heated jet and self-excited hot jet (20 ns exposure time; length of 'T' mark = jet width). (*a*) Slightly heated jet with $S = 0.95$, $q_j = 1.31$ mmH_2O; (*b–d*) hot jet with $S = 0.73$, $q_j = 1.31$ mmH_2O.

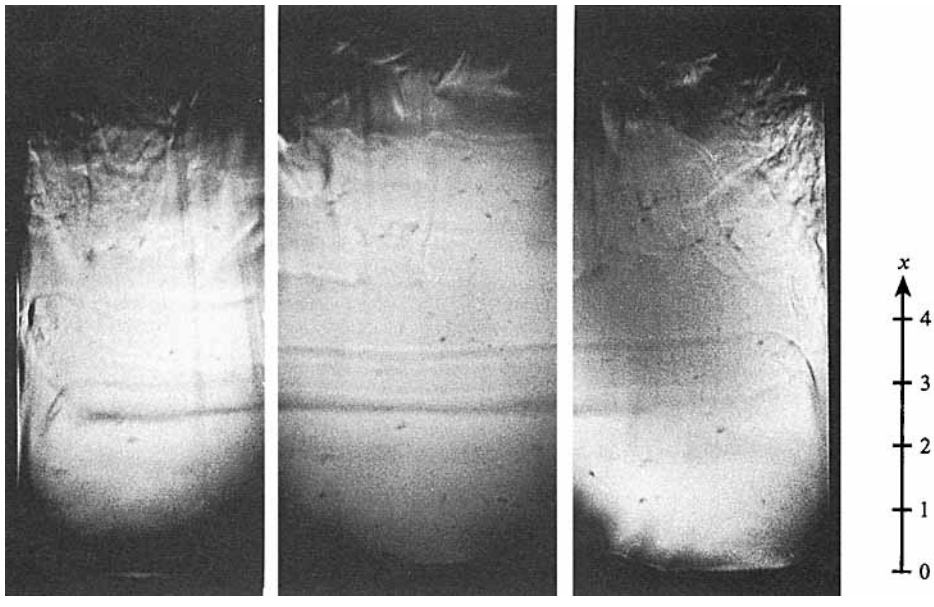

FIGURE 19. Side view of the heated jet with $S = 0.75$ and $q_j = 1.30\ \mathrm{mmH_2O}$.

obtained from the bicoherence are not sensitive to the value of b_n^2, as long as it is negative and not too large as in figure 14, such that one can set $b_n^2 = 0$ in most instances.

In summary, the bicoherence allows an accurate and rather noise-tolerant detection of the onset of self-excited behaviour and yields results that are fully consistent with the $S_{crit} \approx 0.92$ obtained from figures 12 and 13. Finally it is noted that the experimental value of $S_{crit} \approx 0.92$ for the Hopf bifurcation to a global mode lies below the value of $S = 0.95$ for the appearance of absolute instability in the linear theory. This is, as in the two-dimensional wake, in agreement with the results of the model study by Chomaz *et al.* (1991), which showed that global instability only develops when a sufficient region of the flow field is absolutely unstable on a locally parallel basis. The heated two-dimensional jet is therefore another illustration for the usefulness of linear stability theory in predicting global characteristics.

3.4. *Flow visualization and the jet spreading*

The schlieren images of figure 18, focused at $z = 0$, illustrate the qualitative difference of the vortex structure in the near field of a slightly heated jet with $S = 0.95$ and a hot jet with $S = 0.73$. In the former case, vortices in the shear layers evolve gradually from small wavy structures to larger and larger vortex pairs. In the hot jet, on the other hand, large vortex-pair structures form immediately after an initial, virtually undisturbed jet region, as illustrated by different schlieren images on figure 18(*b–d*) taken under the same hot conditions. On all the images the 'T'-mark at the base has a height and width of one jet width to provide a reference. It was, together with the 'x-axis', attached to the transparent end plates of the jet. These large vortex structures are found to be symmetric about the jet centreline, corresponding to the varicose instability mode as suggested by the theoretical investigation of Yu & Monkewitz (1990). A composite side-view schlieren image is shown on figure 19 to document the two-dimensional characteristics of the vortex pairs near the nozzle. It shows that the hot-

jet oscillations under consideration remain two-dimensional (except near the end plates) up to approximately $x = 4$, where three-dimensional disturbances seem to become important. This observation implies that the first strong vortex pair is essentially two-dimensional since it forms at $x < 4$.

Monkewitz *et al.* (1989) observed the spectacular spreading of an axisymmetric hot jet undergoing limit-cycle oscillations. In this study, it has been shown from mean flow data that the two-dimensional hot jet also spreads somewhat more or earlier than the cold jet. To obtain more information about the spreading of the two-dimensional jet, the jet cross-sections were visualized. Cross-sectional views at $x = 1$–7 are shown on figures 20 and 21 for the cold jet and the hot jet with $S = 0.76$, respectively. Beginning at $x = 3$, the hot jet is seen to have a wider cross-section than the cold jet and to develop stronger three-dimensional structures, which appear on figure 21 to be predominantly symmetric with respect to the jet centreline $y = 0$. We also note that vortex cores appear in pairs symmetric around $y = 0$, which further confirms that the large organized structures formed in a self-excited hot two-dimensional jet correspond to the varicose mode.

To describe the jet cross-sections quantitatively, we consider the rather sharp boundary between white and black in the laser cuts, which represents the boundary between seeded jet fluid and unseeded ambient fluid. At each streamwise station between three and six snapshots of the type shown on figures 20 and 21 were taken and the distance of the boundary between jet and ambient fluid from the centreline $y = 0$ was measured as a function of z. Thereby $y^+(z)$ and $y^-(z)$ are defined as the distance from $y = 0$ to the 'upper' and 'lower' boundaries, respectively. In cases where multiple boundaries are observed at one z (at larger x), $y^\pm(z)$ is the sum of the lengths of all the separated white regions, i.e. regions of jet fluid, between $y = 0$ and $y = \pm\infty$ (z fixed). The boundaries y^+ and y^- of the laser images are then digitized at intervals of $\Delta z = L/105$, where L is the length of the two-dimensional jet nozzle, and normalized by the jet width.

The overall mean values with respect to z of the boundary, $\bar{y} = \frac{1}{2}(|\bar{y}^+| + |\bar{y}^-|)$, which is a function of x, are shown on figure 22(*a*), with error bars representing the standard deviation of the three to six samples used for this figure. It illustrates the spreading of the two-dimensional jet in the streamwise direction and shows that the difference between hot and cold jets lies mostly in the earlier spreading of the hot jet between $x = 2$ and 5. The averaged r.m.s. values of y^+_{rms} and y^-_{rms}, denoted as y_{rms}, are shown on figure 22(*b*). The higher values of the y_{rms} for the hot jet indicate a trend to a more convoluted interface in the self-excited hot jet, which implies more mixing with the ambient fluid and is consistent with the earlier decay of centreline velocity on figure 7.

To quantify the symmetry of the cross-sections, the correlation C between the boundaries on both sides, defined as

$$C = \frac{1}{y^+_{rms} y^-_{rms}} \frac{1}{L} \int_{-L/2}^{L/2} y'^+ y'^- \, \mathrm{d}z, \tag{9}$$

is computed, where $y'^\pm = y^\pm - \bar{y}^\pm$. If y^+ and y^- are fully correlated, $|C| = 1$ with $C = 1$ and $C = -1$ corresponding to perfect symmetry and antisymmetry about $y = 0$, respectively.

The values of the correlation obtained from the cross-sectional views are shown on figure 22(*c*). The correlations are found to be positive for both the cold and the hot jet, with consistently higher values of C in the hot case, except at $x = 1$ where y_{rms} is small and the error is large. This confirms the visual impression of symmetric three-dimensional structures in a self-excited hot jet in particular. No clear periodicity in z

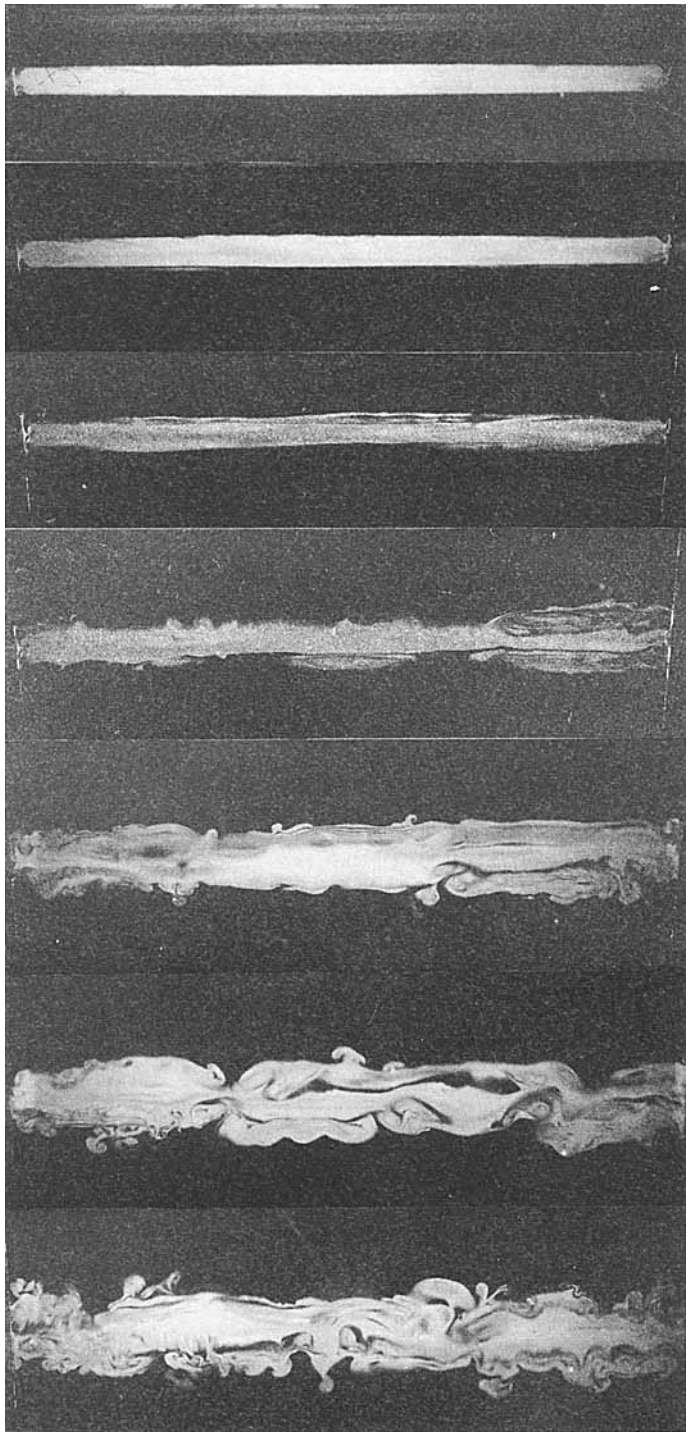

FIGURE 20. Cross-sectional views of the cold jet with $q_j = 1.25$ mmH_2O, at $x = 1, 2, 3, 4, 5, 6, 7$ (from top to bottom).

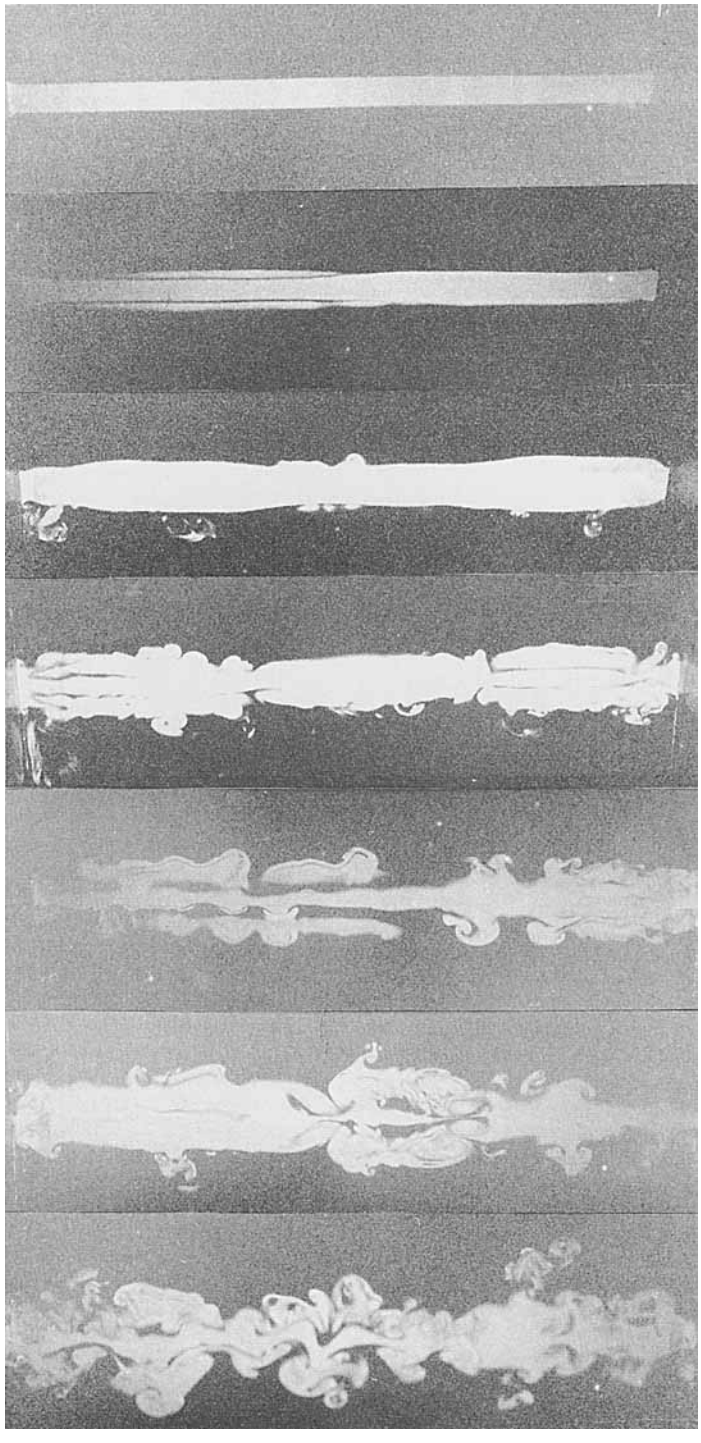

FIGURE 21. Cross-sectional views of the hot jet with $S = 0.76$ and $q_j = 1.25$ mmH_2O, at $x = 1, 2, 3, 4, 5, 6, 7$ (from top to bottom).

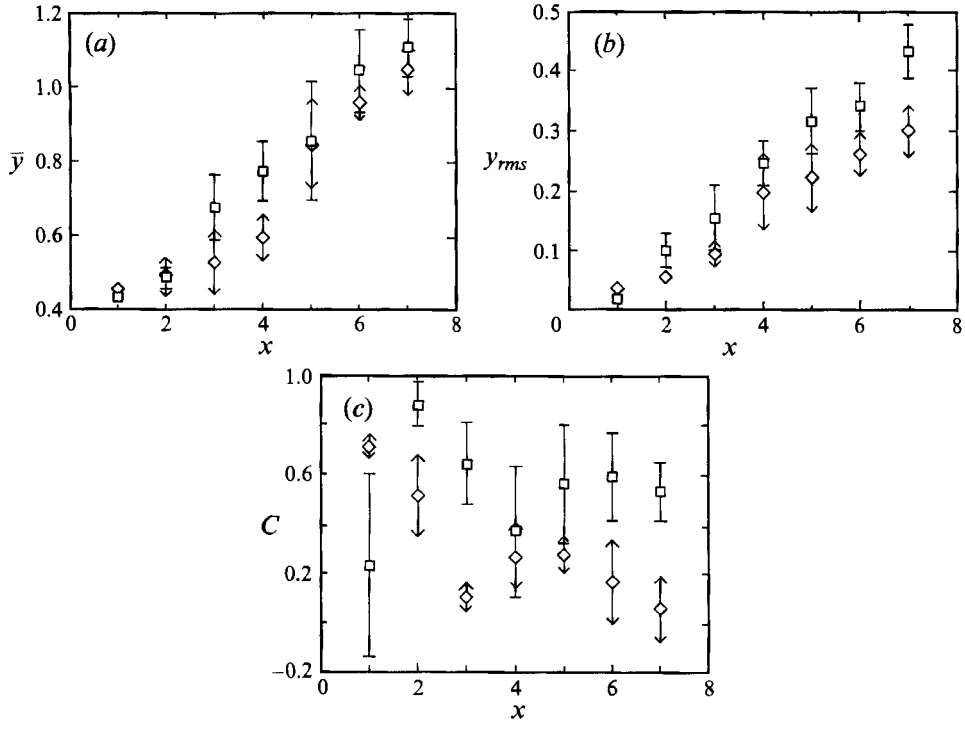

FIGURE 22. (*a*) The mean value $\bar{y}$, (*b*) the r.m.s. value y_{rms} (all lengths made non-dimensional with H), and (*c*) the correlation, versus the streamwise coordinate, estimated from cross-sectional views for the cold jet (◇) and for the hot jet (□) with $S = 0.76$. $q_j = 1.25$ mmH_2O in both cases.

can be detected, however, partly because the aspect ratio of the jet may not be sufficiently large for this purpose.

4. Conclusions

A heated two-dimensional air jet with aspect ratio of 20:1 has been shown to perform self-excited oscillations when the density ratio S is below 0.9 much in the same way as an axisymmetric jet below $S \approx 0.7$. These oscillations represent a limit cycle which is reached through a Hopf-bifurcation at $S_{crit} \approx 0.9$. Below S_{crit}, the self-excited oscillations with a primary Strouhal number based on jet width of $St = fH/u_j \approx 0.32$, which is significantly lower than the Strouhal number of the most amplified initial shear-layer mode, dominate the whole near field of the hot jet. These results are confirmed by measurements of bicoherence, which show that the primary frequency and its subharmonic are phase-locked when the density ratio is below the critical value S_{crit}. It has also been shown that bicoherence is superior to amplitude spectra for the determination of the critical parameter S_{crit} because it is noise tolerant, i.e. because it filters out the uncorrelated spectral contributions due to noise. As a consequence, at S_{crit} the bicoherence drops much more abruptly to zero than the peaks of the amplitude spectrum.

At this point the comparison between these experimental findings and theoretical results needs to be addressed. Attempts to predict the linear global frequency from the analysis of global modes (Monkewitz *et al.* 1993) have been unsuccessful so far. The main reason is that the current analysis can only handle cases where the global

behaviour is dominated exclusively by either a saddle point of the absolute growth rate or by the flow boundary, while the hot jet under consideration is found to be dominated by both. In other words, the frequency of the jet oscillations is influenced by both the region next to the nozzle and the region around the profile with the largest absolute growth rate, where the jet shear layer has a vorticity thickness of approximately 14% of H (figure 3*a* of Yu & Monkewitz 1990).

One pair of large vortices was observed in the near-field region of the self-excited jet, providing evidence of vortex pairing between the jet nozzle and the end of the potential core. The strength of this large vortex pair and the enhanced three-dimensional disturbances in the self-excited hot jet lead to a larger spreading than in the uniform-density jet. The better organization of the vortex pairs is also seen on the mean temperature profiles, which show plateaux in the jet shear layers corresponding to the mixed vortex cores. However, the spreading is found to be not as spectacular as in the axisymmetric case and in particular no side jets were observed. The reason for this marked difference can only be speculated upon at this time as the mechanism for the formation of side jets in the axisymmetric case is not fully understood. If the hypothesis put forward by Monkewitz & Pfizenmaier (1991) is correct – that the side-jets are the direct result of a strong and organized instability of the vortex rings – the following may explain the difference to the two-dimensional case. In the axisymmetric case the number of waves on a vortex ring must be an integer (typically around 5) because of the periodic boundary conditions in the azimuthal direction. This number of waves depends on the ratio of vortex core to vortex ring diameter (Widnall, Bliss & Tsai 1974), and must remain constant for small variations of jet flow parameters and external noise characteristics. Therefore the azimuthal structure of vortex rings in an axisymmetric jet is thought to be relatively clean and stable, leading to pronounced nonlinear effects, namely the side jets.

In the two-dimensional jet, on the other hand, no periodic boundary conditions apply in z and a continuum (in the limit of infinite jet aspect ratio) of three-dimensional disturbances with different wavelengths (in z) are equally likely to grow (see for instance Pierrehumbert & Widnall 1982). We therefore hypothesize that it is the lack of organization of the three-dimensional disturbances and possibly the lack of perfect symmetry documented on figure 22(*c*) which prevents the formation of side jets in the two-dimensional jet.

The financial support for this research by the Air Force Office of Scientific Research under Grants No. 87-0329 and No. 89-0421 is gratefully acknowledged.

REFERENCES

CHOMAZ, J. M., HUERRE, P. & REDEKOPP, L. G. 1991 A frequency selection criterion in spatially developing flows. *Stud. Appl. Maths* **84**, 119–144.

DRAZIN, P. G. & REID, W. H. 1981 *Hydrodynamic Stability*. Cambridge University Press.

HANNEMANN, K. & OERTEL, H. 1989 Numerical simulation of the absolutely and convectively unstable wake. *J. Fluid Mech.* **199**, 55–88.

HO, C. M. & HSIAO, F. B. 1982 Evolution of coherent structures in a lip jet. In *Structure of Complex Turbulent Shear Layers* (ed. R. Dumas & L. Fulachier), pp. 121–136. Springer.

HO, C. M. & HUERRE, P. 1984 Perturbed free shear layers. *Ann. Rev. Fluid Mech.* **16**, 365–424.

HUERRE, P. & MONKEWITZ, P. A. 1990 Local and global instabilities in spatially-developing flows. *Ann. Rev. Fluid Mech.* **22**, 474–537.

KIM, Y. C. & POWERS, E. J. 1979 Digital bispectral analysis and its application to nonlinear wave interactions. *IEEE Trans. Plasma Sci.* **PS-7**, 120–131.

KNISELY, C. & ROCKWELL, D. 1982 Self-sustained low-frequency components in an impinging shear layer. *J. Fluid Mech.* **116**, 157–186.

KYLE, D. & SREENIVASAN, K. R. 1989 Stability properties of He/air jets. In *Forum on Chaotic Dynamics, ASME Fluids Engng Spring Conf. July 10–12, Le Jolla, CA.*

LIEPMANN, H. W. & ROSHKO, A. 1957 *Elements of Gasdynamics.* Wiley.

MIKSAD, R. W., JONES, F. L., KIM, Y. C. & KHADRA, L. 1982 Experiments on the role of amplitude and phase modulations during transition to turbulence. *J. Fluid Mech.* **123**, 1–29.

MIKSAD, R., JONES, F. & POWERS, E. 1983 Measurements of nonlinear interactions during natural transition of a symmetric wake. *Phys. Fluids* **26**, 1402–1409.

MONKEWITZ, P. A., BECHERT, D. W., BARSIKOW, B. & LEHMANN, B. 1990 Self-excited oscillations and mixing in a heated round jet. *J. Fluid Mech.* **213**, 611–639.

MONKEWITZ, P. A. & HUERRE, P. 1982 Influence of the velocity ratio on the spatial instability of mixing layers. *Phys. Fluids* **25**, 1137–1143.

MONKEWITZ, P. A., HUERRE, P. & CHOMAZ, J. M. 1993 Global linear stability analysis of weakly non-parallel shear flows. *J. Fluid Mech.* **251**, 1–20.

MONKEWITZ, P. A., LEHMANN, B., BARSIKOW, B. & BECHERT, D. W. 1989 The spreading of self-excited hot jet by side jets. *Phys. Fluids* A **1**, 446–448.

MONKEWITZ, P. A. & PFIZENMAIER, E. 1991 Mixing by 'side jets' in strongly forced and self-excited round jets. *Phy. Fluids* A **3**, 1356–1361.

MONKEWITZ, P. A. & SOHN, K. D. 1986 Absolute instability in hot jets and their control. *AIAA Paper* 86-1882.

MONKEWITZ, P. A. & SOHN, K. D. 1988 Absolute instability in hot jets. *AIAA J.* **26**, 911–916.

OPPENHEIM, A. V. & SCHAFER, R. W. 1975 *Digital Signal Processing.* Prentice-Hall.

PIERREHUMBERT, R. T. & WIDNALL, S. E. 1982 The two- and three-dimensional instabilities of a spatially periodic shear layer. *J. Fluid Mech.* **114**, 59–82.

PROVANSAL, L., MATHIS, C. & BOYER, L. 1987 Bénard–von Kármán instability: transient and forced regimes. *J. Fluid Mech.* **182**, 1–22.

RAGHU, S. & MONKEWITZ, P. A. 1991 The bifurcation of a hot round jet to limit-cycle oscillations. *Phys. Fluids* A **3**, 501–503.

SREENIVASAN, K. R., RAGHU, S. & KYLE, D. 1989 Absolute instability in variable density round jets. *Exps Fluids* **7**, 309–317.

WIDNALL, S. E., BLISS, D. B. & TSAI, C.-Y. 1974 The instability of short waves on a vortex ring. *J. Fluid Mech.* **66**, 35–47.

YU, M.-H. & MONKEWITZ, P. A. 1990 The effect of nonuniform density on the absolute instability of two-dimensional inertial jets and wakes. *Phys. Fluids* A **2**, 1175–1181.